How to cite: Angew. Chem. Int. Ed. 2024, e202319702
doi.org/10.1002/anie.202319702

Photochemistry

Significance of Vibronic Coupling that Shapes Circularly Polarized Luminescence of Double Helicenes

*Tadashi Mori**

Abstract: The circularly polarized luminescence (CPL) spectra of *S*- and *X*-shaped double helicenes exhibit distinct vibrational structures and overall shape variations. In this study, we conducted an in-depth investigation into the vibronic effects influencing the CPL spectra of two double helicenes, namely **DPC** and **DNH**. Employing state-of-the-art computations utilizing the FC-HT$_1$|VH model at the CAM–B3LYP/def2-TZVP level, we unveiled the paramount impact of Franck–Condon (FC), Herzberg-Teller (HT), and Duschinsky effects on their chiroptical responses. Our research underscores the pivotal role of structural deformations associated with the S_1-to-S_0 electronic transition in molding CPL spectra and wavelength-dependent dissymmetry (g) factor values, as well as the significance of HT effects in shaping and enhancing CPL responses. This extensive investigation not only advances our comprehension of the vibronic characteristics in configurationally distinct double helicenes but also offers valuable insights for the design of chiral molecules featuring controllable or finely-tunable CPL responses.

Introduction

Helicenes, characterized by their *ortho*-annulated extended aromatic structure and distinctive spiral configuration, are known for their unique photophysical properties.[1,2,3] They possess a stable helical chirality, either left-handed (minus, *M*) or right-handed (plus, *P*), which has attracted significant interests, primarily due to their remarkable chiroptical responses, including optical rotation (OR), circular dichroism (CD), and circularly polarized luminescence (CPL).[4,5] This characteristic makes them valuable particularly in the field of chiral photonics.[6,7] Surprisingly, the structure of helicenes is more dynamic than originally assumed. The spring-like behavior of helicenes has been verified through a comparison of crystal structures. For instance, the relative angle between terminal thiophene rings in helicenediol significantly depends on hydrogen bonding mode, with an observed angle of 38° in ethanol, increasing to 55° in 1,2-dichloroethane.[8] Smaller helicenes, like carbo[5]helicene, can readily racemize under ambient conditions, and extensive investigations have explored the enantiomerization of a series of carbo[*n*]helicenes.[9] Helicenes have been proposed as potential molecular springs, with relevance to the development of molecular machines. Notably, their photophysical properties can be progressively altered by applying external pressure, leading to the contraction of the helical pitch.[10] Hexa-peri-hexabenzo[7]helicene, featuring a larger helical diameter, also exhibits an intriguing extension-contraction motion, with a considerably lower force constant.[11] Recent advancements have demonstrated the ability to control contraction-extension movements in heterohelicenes using chemical and/or light stimuli.[12] However, these dynamic properties, along with other vibronic contributions, have rarely been considered in discussions of the (chir)optical properties, particularly CPL, of helicenes. Although pioneering work on vibronic effects in helicenes has provided valuable insights through phenomenological considerations related to spectral shape[13,14] and wavelength,[15,16] an importance of symmetry of helicenes on the vibronic effects remains elusive. Exciting potential for further exploration in this domain persists.

In this study, we explore the vibronic contributions that influence the CPL spectra of two distinct double helicenes,[17] namely, diphenanthro[3,4-c:3',4'-l]chrysene (**DPC**) and dinaphtho[2,1-i:1',2'-l]hexahelicene (**DNH**).[18] Our aim is to compare and provide a rational explanation for the unique fine structures and shapes of their spectra. While previous pioneering research has explored absorption, emission, and CD spectra for the parent hexahelicene (**HH**) and its derivatives, very limited attention has been given to CPL due to the weak and inconclusive experimental spectra associated with hexahelicenes.[19] Thankfully, in the case of the double helicenes **DPC** and **DNH**, we have the advantage of well-resolved lowest-energy CD bands and CPL spectra with distinctive fine structures. This allows us to critically examine the contributions of Franck-Condon (FC) and Herzberg-Teller (HT) effects,[20,21] as well as the Duschinsky effect,[22,23] in the vibronic interactions related to the electronic transition (vide infra). Our simulations have, for the first time, offered valuable insights into how different symmetries influence the vibronic contributions to the CPL spectra of double helicenes. Notably, we have shown that HT effects, arising from distinct normal modes, significantly

[*] Dr. T. Mori
Department of Applied Chemistry, Graduate School of Engineering, Osaka University
2-1 Yamada-oka, Suita, Osaka, 565-0871, Japan
E-mail: tmori@chem.eng.osaka-u.ac.jp

shape the spectra, thus finely tuning the CPL responses. It is noteworthy that the HT effects exhibit notably greater prominence in CPL when compared to fluorescence spectra. This disparity in significance is attributed to the potential sign inversion induced by the HT contribution in the CPL response, possibly resulting in variations in spectral shape.

Results and Discussion

Comparison of vibronically resolved theoretical CPL spectra with experiment

Over the last three decades, substantial research efforts have been dedicated to the theoretical calculation of chiroptical properties.[24,25] However, the computational study of CPL has been somewhat limited.[26] Such calculations demand in-depth geometric and conformational analyses of the molecule in its excited state, coupled with precise property computations. Besides, previous research in this area has primarily focused on electronic transitions, with relatively little attention given to vibronic effects. To the best of our knowledge, an exploration of vibronic contributions in CPL spectra has been limited to specific studies, including investigations into boron dipyrromethene dyes,[27] camphorquinone, and related ketones.[28,29] Furthermore, the analysis of vibronically resolved CPL spectra of helicenes presents notable challenges, primarily due to the inherently low signal-to-noise ratio in experimental spectra. This results from small dissymmetry factors, typically in the range of 10^{-3} to 10^{-4}, as well as low emission intensity of helicenes. Consequently, the analysis of substituent effects on vibrationally resolved CPL spectra of hexahelicenes has predominantly remained qualitative in nature.[18] In a related computational study of double *BO*-pentahelicene, it was discussed that the mirror symmetry between the CD and CPL spectra breaks down due to the opposing HT effects between these spectra.[30]

The theory for calculating vibronic effects associated with electronic transitions, including absorption, emission, CD, and CPL spectra, has been extensively described in previous study on substituted hexahelicenes.[18] Initially, we employed a methodology that relied on a time-independent (TI) approach. This approach involved computing a weighted sum of transitions between vibrational states associated with the initial and final electronic states, and thus is grounded in the sum-over-states principle, enabling a more thorough analysis of spectra, especially for prominent vibronic bands. Subsequently, we incorporated a time-dependent (TD) approach to enhance the convergence of spectral line shapes with reduced computational time. The vibronic contributions were calculated in harmonic approximation, which also included the Duschinsky effect. The FC and HT contributions were evaluated in these calculations in the limit of first-order perturbation theory as the first and second terms of the Taylor expansion coefficients of the electronic or magnetic transition dipole moment.[31] In previous investigation, the difference between Adiabatic Hessian (AH) and Vertical Hessian (VH) models[32] was thoroughly tested to assess the validity of harmonic approximation and to accurately describe the spectra around the spectral maximum or near 0–0 transitions. In this study, we consistently employed the VH model and the transition electric and magnetic dipole moments are taken at the initial states (i.e., the ground state for CD and the excited state for CPL, respectively), as the method has demonstrated superior performance. These were labeled (as in the previous publication) as $FCHT_0|VH$ or $FCHT_1|VH$ calculations, respectively.

In this study, we adopted the $FC\text{-}HT_1|VH$ model at the CAM–B3LYP/def2-TZVP level to calculate the vibrationally resolved CPL spectra of double helicenes **DPC** and **DNH**, using the *FCclasses3* code.[33] A more detailed account of the computational methodology and additional discussion on other spectra can be found in the Supporting Information. Briefly, the computed spectra using TD calculations accurately replicated the overall appearance of the experimental CPL spectra (in dichloromethane at 25 °C) for both double helicenes, as depicted in Figure 1, top.[17] Remarkably, these computational results proficiently depict the unique spectral characteristics that differentiate the two double helicenes, with the apparent difference arising from multiple factors, including the energy spacing between the vibronic contributions and band broadening. In the case of **DPC**, a significant band was observed in close proximity to the 0–0 band, accompanied by sequential peaks at the shoulders and tail of the principal band. On the other hand, **DNH** exhibited broader bands characterized by intricate fine structures that appeared forked, with the most intense

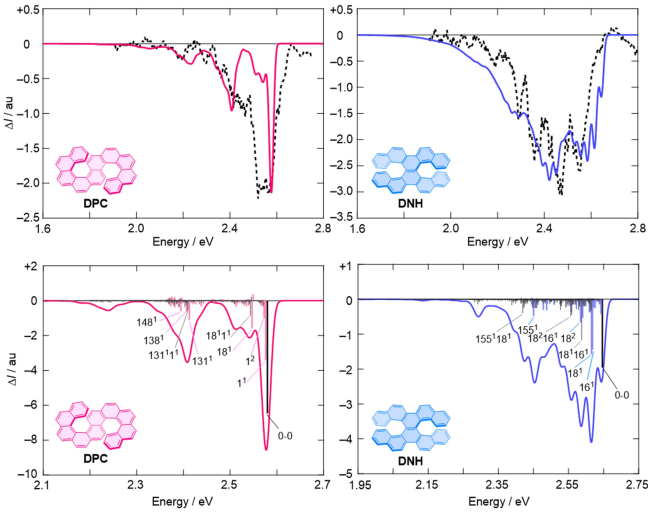

Figure 1. Vibrationally resolved CPL spectra of double helicenes **DPC** and **DNH** calculated by the $FC\text{-}HT_1|VH$ model at the CAM–B3LYP/def2-TZVP level. Top: TD-calculated converged CPL spectra compared with the experiment (dashed lines). Bottom: Assignment of the main stick bands based on TI-calculated spectra. Vibrational contributions labeled as n^a and $n^a m^b$ indicate the normal mode n with its quanta a (red and blue) and the combination band with a and b quanta on modes n and m (grey), respectively. The 0–0 bands are colored in black. The calculated spectrum of **DNH** was red-shifted by 0.7 eV to better match with the experiment. The corresponding fluorescence spectra can be found in Figure S3 in the SI.

peak situated in the middle of these bands. As a result, these distinctions translated into notable variations in dissymmetry factors at different monitoring wavelengths (vide infra). While the FC model on its own effectively captured the spectral shape, it is important to note that the FC contribution represented only 48 % and 32 % of the total intensity in **DPC** and **DNH**, respectively, based on an analysis of HT (I_{tot}^{HT}) and FC+HT ($I_{tot}^{FC} + I_{tot}^{HT}$) total intensities (Table S1 and Figure S4 in the SI). Thus, HT effects indeed play a pivotal role in significantly enhancing the spectral intensity and shaping the overall features of the CPL spectra for **DPC** and **DNH**. Moreover, it is worth noting that the magnitude of $I_{tot}^{|HT|}$ are notably larger than the $|I_{tot}^{HT}|$ values, where $I_{tot}^{|HT|}$ represents the total HT contribution ignoring sign variance, implying that the HT effects induced by different normal modes contribute with opposite sign.

Assignment of main vibronic contributions

The convoluted CPL spectra for the double helicenes **DPC** and **DNH**, which were computed using TI calculations based on the sum-over-state approach, are shown in Figure 1, bottom. The Figure also illustrates strong vibronic stick bands, where the lengths of the bars are proportional to their intensity. These bands are color-coded, with fundamental and overtone bands shown in red or blue, and they are labeled as "n^a". Additionally, combination bands, shown in grey, are denoted by the label "$n^a m^b$," with n and m indicating the normal modes of the ground (S_0) state, while a and b represent the number of quanta. Table 1 provides a summary of the key properties associated with these stick bands, including relevant details such as their vibrational modes and intensities. Furthermore, selected modes are visually represented, allowing for a more comprehensive understanding of the vibrational contributions to the CPL spectra (for larger illustrations and of additional modes, see Figure S5 in the SI). The relative HT contributions in each vibronic band for CPL and fluorescence spectra are quantified using parameters such as I^{HT} / I_{tot}^{HT} or their sign-corrected counterparts, $|I^{HT}| / I_{tot}^{|HT|}$. Additionally, the assessment of contributions in individual vibronic modes includes the provision of displacement factor (δ) and the Duschinsky matrix element (J^2).

We initially focus on *S*-shaped **DPC**, where the TI approach also provided a well-converged spectrum. The most prominent band emerges at a high energy of approx-

Table 1: Physical characteristics of selected vibrational modes relevant for the vibronic structures of the CPL spectra of double helicenes **DPC** and **DNH**.[a]

Helicene	S_0 mode (ω /cm^{-1})	Assignment	I^{HT}/I_{tot}^{HT} (CPL, %)	$\lvert I^{HT}\rvert/I_{tot}^{\lvert HT\rvert}$ (CPL, %)	I^{HT}/I_{tot}^{HT} (FL, %)	δ	S_1 mode (ω' /cm^{-1})	J^2
DPC	1 (27.0)	helical wagging	0.7	0.2	0.1	1.12	1 (28.6)	1.00
	18 (255.3)	helical twisting	0.5	0.2	1.6	0.36	18 (263.3)	0.83
							19 (271.6)	0.14
	131 (1322)	C=C stretching, C–H rocking	0.5	0.2	0.01	−0.21	131 (1322)	0.54
							129 (1312)	0.19
							134 (1374)	0.09
	138 (1401)	C=C stretching, C–H rocking	2.0	0.6	0.8	−0.48	141 (1401)	0.58
							134 (1374)	0.27
	148 (1491)	C=C stretching, C–H rocking, scissoring	16.0	5.1	2.8	−0.00002	147 (1491)	0.99
DNH	16 (219.7)	helical stretching	0.8	0.7	2.6	1.02	16 (226.8)	0.99
	18 (240.5)	helical twisting	0.01	0.01	0.05	1.30	18 (250.0)	1.00
	155 (1572)	C=C stretching, C–H rocking	17.0	14.0	14.4	0.21	155 (1582)	0.95

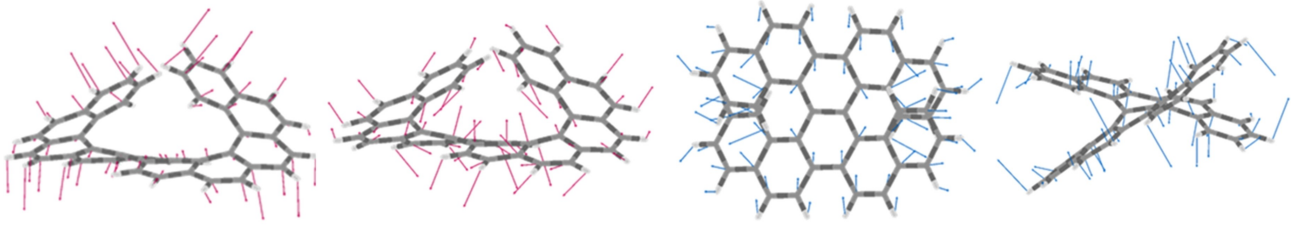

#1 (**DPC**) #18 (**DPC**) #16 (**DNH**) #18 (**DNH**)

[a] Contribution of each mode to the total (absolute) HT intensities (I^{HT}/I_{tot}^{HT} and $|I^{HT}|/I_{tot}^{|HT|}$), its displacement in dimensionless units (δ), and the square of the Duschinsky matrix element representing a projection of the mode ω' of S_1 state on the mode ω of S_0 state (J^2). Selected vibrational modes are illustrated at the bottom. Refer to Figure S5 in the Supporting Information for larger figures and additional vibrational modes.

imately 2.6 eV and encompasses the 0–0 band along with the fundamental and overtone bands originating from normal mode #1. This particular band is attributed to helical wagging motion with a very low harmonic frequency of 27 cm^{-1} (Table 1). While the sign is the same, the contributions of the vibronic fundamental and overtone bands 1^1 and 1^2 to the CPL intensity are notably weaker compared to that of the 0–0 band, leading to an apparent discrepancy between the calculated and experimental dissymmetry factors at the 0–0 energy transition and CPL emission ($g_{0\text{-}0}$ and/or g_{CPL}) for this double helicene. The fundamental band of the low-frequency mode #18 (255 cm^{-1}), which is associated with helical twisting, and its combination band, contribute to forming the shoulder of the first band. Significantly, all of these bands are HT active. While the modes 1 and 18 of the ground (S_0) state are primarily projected onto the same modes of the excited (S_1) state, they are considerably displaced during the electronic transition. The second band, which peaks at around 2.4 eV and is experimentally observed as a shoulder of the main peak, exhibits emission intensity comparable to that of the first band but is less significant in the CPL response. This band mainly comprises the fundamentals of modes #131, #138, and #148, which are attributed to C=C stretching, combined with C–H rocking or scissoring motion, with harmonic frequencies of 1322, 1401, and 1491 cm^{-1}, respectively. Remarkably, the HT contribution of mode #148 was found to constitute as much as 16 % of the total HT component of CPL intensity. The third band around 2.2–2.3 eV seems to be composed of many minor vibronic contributions, which, however, reproduces the experimental CPL behavior well. In a word, the CPL response for **DPC** is primarily governed by the contribution of the 0–0 band, leading to the CPL peak occurring at the high-energy edge of the entire band. However, the intensity of this peak is somewhat diminished by the low-frequency vibronic bands associated with the helical wagging mode. Consequently, it is hypothesized that the suppression of this vibrational mode in this *S*-shaped double helicene structure, by structural modification and/or supramolecular strategy (e.g., confinement or crystal engineering), could lead to a substantial amplification of the CPL response.

Now, let us turn our attention to the spectrum of the *X*-shaped **DNH**. In the experimental CPL spectrum, we observe two main bands with additional vibronic progression, followed by additional shoulder peaks. In this case, the calculated spectrum using the TI method was less well-converged compared to **DPC**. It is noteworthy that, while the second band was the most intense in the experimental spectrum, the first band became the strongest in the computed spectrum using the TI method. In fact, the overall shape of the TI spectrum more closely resembles that of the FC|VH TD spectrum (see Figure S4 in the SI), and the relative intensity of each band is better recovered when HT effects are incorporated, as in the FC-HT_1|VH method. However, identifying the vibronic origins of these bands was relatively straightforward due to the consistent and clear energy spacing of around 0.2 eV between them. In the calculation, the 0–0 band is again the strongest in the stick spectrum, but the spectral maximum appears at a lower energy of around 2.6 eV. This maximum is composed of fundamentals and overtones of modes #16 and #18, along with their combination bands. The two low-frequency modes (220 and 241 cm^{-1}) originate from a collective motion of the helical structure and are primarily assigned as helical stretching and twisting motions, respectively (Table 1). It is essential to highlight that these modes in **DNH** are fundamentally different from the helical wagging mode that plays a crucial role in *S*-shaped **DPC**. In **DNH**, the CPL peak appears nearly in the middle of the bands (second band) and is composed of mode #155 and its combination band with mode #18. The mode #155 (1572 cm^{-1}) represents a combination of C=C stretching and C–H rocking vibrations, with HT contributing significantly, up to 17 % of the total HT intensity. Notably, this band serves as the spectral maximum in both experimental and well-converged TD-calculated spectra. All these vibronic bands in **DNH** are HT active, involving substantial displacements during the electronic transition. Consequently, unlike **DPC**, the vibrational mode of the aromatic ring and its HT contribution are pivotal in enhancing the CPL response of **DNH**.

Wavelength dependence of dissymmetry (g) factors

In the pursuit of designing CPL-active molecules in materials chemistry and enhancing our understanding of chiral materials for diverse technological applications, the dissymmetry (g) factor and quantum yield of emission stand out as crucial parameters.[34,35] The g factor of CPL directly quantifies molecular chirality (see also additional discussion in the SI) and is closely linked to the chiral characteristics of the emitting molecule and its environment in the excited state. The g factor is defined as the difference in emission intensity between left-handed (I_L) and right-handed (I_R) polarized light, divided by the averaged light intensity at a given frequency:[36]

$$g = \frac{I_L - I_R}{\frac{1}{2}(I_L + I_R)}$$

This parameter, however, presents a greater challenge in terms of enhancement and precise control. In practical terms, due to the difficulties presented by CPL spectra with a low signal-to-noise ratio, values are often reported at the peaks of maximum CPL intensity, lacking detailed wavelength dependence information. However, it is consistently observed that the CPL intensity and the g factor attain their peaks at frequencies distinct from the maximum fluorescence intensity. This observation implies that the g factor is affected by the emission energy (due to distinct origin), and consequently, the specific frequency dependence of the g factor offers additional insights into the chirality of the molecule in its excited state. While the common explanation for such differences in peak positions involves varying experimental conditions (e.g., bandwidth, etc.) between CPL and fluorescence measurements, it is important to recognize that other factors, such as the

vibronic effect, the central focus of this study, can more seriously contribute to these discrepancies.

Certainly, the comparison of spectral maxima becomes particularly crucial in the context of vibronically resolved spectra. Even a slight error can result in the shift of the maximum band, causing the alignment between the experimental and calculated peaks to deviate from the same vibronic peak. Consequently, our analysis encompasses the comparison of *g* factor values at the peaks of fluorescence emission (g_{FL}) and CPL emission (g_{CPL}), as well as at the 0–0 energy transition ($g_{0\text{-}0}$), as elaborated in Table 2. Theoretical $E_{0\text{-}0}$ energies for emission were overestimated by around 0.4 eV. Consequently, the reported values were adjusted to enable a direct comparison with the experimental results. Our computation using the FC-HT$_0$|VH model for **DNH** successfully reproduced the experimental *g* factor values at all three frequencies. Notably, the experimental data showcased the largest (absolute) *g* value at the CPL maximum, followed by the 0–0 energy and the fluorescence maximum. Impressively, this pattern was also accurately captured by our calculation. In the case of **DPC**, however, the agreement between computational and experimental *g* factor was less satisfactory, particularly when evaluating $g_{0\text{-}0}$ and g_{CPL} values. It is to note that in the computation, the peak of maximum CPL emission coincides with the 0–0 band. The observed discrepancy primarily stems from a prominent low-frequency vibrational mode (as mentioned earlier), which remains unresolved in the experiment. Conversely, the calculation treated the *g* factor values at the 0–0 band and other vibronic bands as separate entities, potentially leading to the disagreement.

When comparing the two double helicenes, **DPC** and **DNH**, notable differences were observed in the *g* factor variations. Specifically, at the CPL maximum, **DNH** exhibited a larger *g* factor than **DPC**, whereas **DPC** showed a more favorable value at the fluorescence maximum. At the 0–0 band, the *g* factor value was comparable or slightly greater in **DPC**. Importantly, our simulations effectively replicated these trends, considering an overlap of 0–0 and vibronic bands of #1 in **DPC**. Such distinct behavior arises from the considerable frequency separation between the maximum and the 0–0 band in **DNH**, a unique characteristic of this particular double helicene. It is worth noting that while previous studies on substituted helicenes attributed the less satisfactory agreement between experimental and calculated *g* factors to the overestimation of HT effects,[18] this factor does not appear to be the primary cause in the case of the current double helicenes.

Table 2: Comparison of experimental and calculated CPL transition energies and dissymmetry factors of double helicenes **DPC** and **DNH** of different origin.[a]

Helicene	Source	$E_{0\text{-}0}$ /eV	10^3 $\times g_{0\text{-}0}$	E_{FL} /eV	10^3 $\times g_{FL}$	E_{CPL} /eV	10^3 $\times g_{CPL}$	Stokes Shift /cm^{-1}
DPC	exp	2.88	−2.6	2.86	−2.2	2.81	−2.4	210
	calcd	2.92	−6.7	2.76	−3.6	2.92	−6.7	450
DNH	exp	2.58	−2.4	2.51	−1.5	2.47	−3.2	670
	calcd	2.64	−2.3	2.59	−2.3	2.42	−2.9	250
HH	exp	3.00	−0.5	2.95	−0.9	2.95	−0.9	580
	calcd	3.08	−5.4	2.88	+1.2	3.03	−1.3	170

[a] Energies and dissymmetry factors at the 0–0 transition and the peak wavelength in the fluorescence ($_{FL}$) and CPL ($_{CPL}$) spectra for the (*P*,*P*)- or (*P*)-enantiomer. The experimental 0–0 energy ($E_{0\text{-}0}$) was estimated using the absorption fluorescence crossing point (AFCP) method. Calculated excitation energies were 0.35 eV red-shifted to facilitate a direct comparison.

Conclusion

In summary, we have applied the first principle calculations to investigate the vibronic structure of CPL spectra for two double helicenes **DPC** and **DNH**. While the CPL intensities (maximal dissymmetry factors) of these helicenes are comparable, their overall spectral shapes with vibronic progressions exhibit notable differences. Our calculations, conducted using the FC-HT$_1$|VH model at the CAM–B3LYP/def2-TZVP level, have unveiled that the FC contribution plays a fundamental role in shaping the CPL spectra, while the HT contribution primarily governs the intensity of the CPL responses. Specifically, in the case of the *S*-shaped **DPC**, the CPL response is predominantly shaped by the 0–0 band, resulting in the CPL peak appearing at the high-energy edge of this band. The intensity of this peak is substantially reduced by the presence of low-frequency vibronic bands associated with the helical wagging mode #1 with a harmonic frequency of 27 cm^{-1}. In contrast, for the *X*-shaped **DNH**, the CPL peak is situated nearly in the middle of the entire bands. This is notably influenced by mode #155, which is associated with aromatic C=C stretching and C–H rocking of entire helicene with a harmonic frequency of 1572 cm^{-1}. This mode plays a crucial role in enhancing the CPL response in **DNH**, with a significant HT contribution of as much as 17 % of the total HT intensity. This first detailed investigation of the vibronic features of CPL spectra in configurationally distinct double helicenes underscores the significance of structural deformations associated with the S_1-to-S_0 electronic transition in shaping the CPL spectra and the wavelength-dependent dissymmetry factor values. Thus, in future endeavors aimed at the design of CPL-responsive molecular systems, particularly in the context of rigid π-systems, the incorporation of vibronic structural considerations will prove to be an integral and indispensable component for the precise fine-tuning and optimization of chiroptical properties.

Supporting Information

The following files are available free of charge. Computational details, additional discussion, spectra, and Figures (PDF)

Acknowledgements

This work was financially supported by Challenging Exploratory Research (JSPS, KAKENHI, Grant Number JP22K19029), by CREST (JST, Grant Number JPMJCR2001), and by the Cooperative Research Program of Network Joint Research Center for Materials and Devices. We are grateful to Professor Javier Cerezo for providing us helpful technical information.

Conflict of Interest

The authors declare no conflict of interest.

Data Availability Statement

The data that support the findings of this study are available in the supplementary material of this article.

Keywords: double helicenes · vibronic emission spectra · Franck-Condon effect · Herzberg-Teller effect · Duschinsky effect

[1] J. Crassous, I. G. Stará, I. Starý, Eds., *Helicenes: Synthesis, Properties and Applications*, Wiely-VCH, Weinheim, Germany, **2022**.
[2] Y. Shen, C.-F. Chen, *Chem. Rev.* **2012**, *112*, 1463–1535.
[3] R. H. Martin, *Angew. Chem. Int. Ed.* **1974**, *13*, 649–660.
[4] M. Cei, L. Di Bari, F. Zinna, *Chirality* **2023**, *35*, 192–210.
[5] W.-L. Zhao, M. Li, H.-Y. Lu, C.-F. Chen, *Chem. Commun.* **2019**, *55*, 13793–13803.
[6] J. R. Brandt, F. Salerno, M. J. Fuchter, *Nat. Chem. Rev.* **2017**, *1*, 0045.
[7] Y. Zhang, S. Yu, B. Han, Y. Zhou, X. Zhang, X. Gao, Z. Tang, *Matter* **2022**, *5*, 837–875.
[8] K. Tanaka, H. Osuga, Y. Kitahara, *J. Chem. Soc. Perkin Trans. 2* **2000**, 2492–2497.
[9] R. Ravat, *Chem. Eur. J.* **2021**, *27*, 3957–3967.
[10] J. Liang, C.-W. Ju, W. Zheng, M. Wagner, Z. Qiu, T. Weil, K. Müllen, *ChemRxiv preprint* **2021**, DOI: 10.26434/chemrxiv-2021-w3r3j.
[11] Y. Nakakuki, T. Hirose, K. Matsuda, *J. Am. Chem. Soc.* **2018**, *140*, 15461–15469.
[12] P. Karaka, J. Choudhury, *Chem. Sci.* **2022**, *13*, 11163–11173.
[13] Y. Liu, Q. Xu, L. Liu, L. Wang, D. He, X. Zhuang, M. Wang, *Spectrochim. Acta Part A* **2021**, *249*, 119293.
[14] Y. Liu, Q. Xu, J. Sun, L. Wang, D. He, M. Wang, C. Yang, *Spectrochim. Acta Part A* **2020**, *239*, 118475.
[15] Q. Xu, Y. Liu, N. Lin, X. Zhao, D. He, L. Wang, Y. Xu, M. Wang, *Dyes Pigm.* **2022**, *204*, 110407.
[16] Q. Xu, L. Chi, Y. Liu, Q. Li, S. Chen, M. Wang, *J. Lumin.* **2021**, *239*, 118374.
[17] T. Mori, *Chem. Rev.* **2021**, *121*, 2373–2412.
[18] H. Tanaka, M. Ikenosako, Y. Kato, M. Fujiki, Y. Inoue, T. Mori, *Commun. Chem.* **2018**, *1*, 38.
[19] Y. Liu, J. Cerezo, G. Mazzeo, N. Lin, X. Zhao, G. Longhi, S. Abbate, F. Santoro, *J. Chem. Theory Comput.* **2016**, *12*, 2799–2819.
[20] G. Herzberg, E. Teller, *Z. Phys. Chem.* **1933**, *B21*, 410–446.
[21] S. H. Lin, H. Eyring, *Proc. Natl. Acad. Sci. USA* **1974**, *71*, 3802–3804.
[22] F. Duschinsky, *Acta Physicochim. URSS* **1937**, *7*, 551–566.
[23] G. J. Small, *J. Chem. Phys.* **2003**, *54*, 3300–3306.
[24] J. Autschbach, *Chirality* **2009**, *21*, E116–E152.
[25] T. D. Crawford, *Theor. Chem. Acc.* **2006**, *115*, 227–245.
[26] G. Longhi, E. Castiglioni, J. Koshoubu, G. Mazzeo, S. Abbate, *Chirality* **2016**, *28*, 696–707.
[27] Q. Yang, M. Fusè, J. Bloino, *Front. Chem.* **2020**, *8*, 801.
[28] B. Pritchard, J. Autschbach, *ChemPhysChem* **2010**, *11*, 2409–2415.
[29] V. Barone, A. Baiardi, J. Bloino, *Chirality* **2014**, *26*, 588–600.
[30] Q. Xu, Y. Liu, X. Zhao, S. Chen, Q. Li, M. Wang, C. Yang, *Spectrochim. Acta Part A* **2020**, *231*, 118132.
[31] F. Santoro, D. Jacquemin, *WIREs Comput. Mol. Sci.* **2016**, *6*, 460–486.
[32] While both the initial and the final-state potential energy surfaces are quadratically expanded around their own equilibrium geometries in the AH model, they are expanded around the equilibrium geometry of the initial state in the VH model. For more details, see refs. [19] and [33].
[33] J. Cerezo, F. Santoro, *J. Comput. Chem.* **2023**, *44*, 626–643.
[34] Y. Nagata, T. Mori, *Front. Chem.* **2020**, *8*, 448.
[35] E. M. Sánchez-Carnerero, A. R. Agarrabeitia, F. Moreno, B. L. Maroto, G. Muller, M. J. Ortiz, S. de la Moya, *Chem. Eur. J.* **2015**, *21*, 13488–13500.
[36] T. Mori, Ed., *Circularly Polarized Luminescence of Isolated Small Organic Molecules*, Springer, Singapore, Republic of Singapore, **2020**.

Manuscript received: December 19, 2023
Accepted manuscript online: February 5, 2024
Version of record online: ■■, ■■

Research Articles

Photochemistry

T. Mori* _____ e202319702

Significance of Vibronic Coupling that Shapes Circularly Polarized Luminescence of Double Helicenes

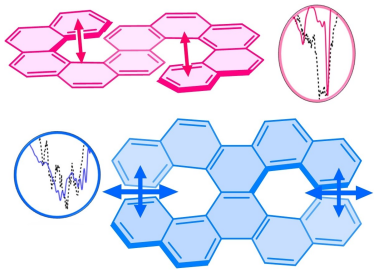

Vibronic coupling shapes the CPL and FL spectra

This study investigates how molecular vibrations influence the circularly polarized luminescence (CPL) of double helicenes **DPC** and **DNH**. It highlights how structural changes during electronic transitions shape CPL spectra and dissymmetry (*g*) factor values, emphasizing the role of Herzberg-Teller effects in enhancing CPL responses.